

Metadata of the chapter that will be visualized in SpringerLink

| | | |
|----------------------|--|--|
| Book Title | Advances in direct methods for materials and structures | |
| Series Title | | |
| Chapter Title | Some Graphical Interpretations of Melan's Theorem for Shakedown Design | |
| Copyright Year | 2018 | |
| Copyright HolderName | Springer International Publishing AG | |
| Corresponding Author | Family Name | Vermaak |
| | Particle | |
| | Given Name | N. |
| | Prefix | |
| | Suffix | |
| | Division | Department of Mechanical Engineering and Mechanics |
| | Organization | Lehigh University |
| | Address | Bethlehem, PA, 18015, USA |
| | Email | vermaak@lehigh.edu |
| Author | Family Name | Boissier |
| | Particle | |
| | Given Name | M. |
| | Prefix | |
| | Suffix | |
| | Division | Department of Mechanical Engineering and Mechanics |
| | Organization | Lehigh University |
| | Address | Bethlehem, PA, 18015, USA |
| | Email | mathilde.boissier@polytechnique.org |
| Author | Family Name | Valdevit |
| | Particle | |
| | Given Name | L. |
| | Prefix | |
| | Suffix | |
| | Division | Department of Mechanical and Aerospace Engineering |
| | Organization | University of California |
| | Address | Irvine, CA, 92697, USA |
| | Email | valdevit@uci.edu |
| Author | Family Name | McMeeking |
| | Particle | |
| | Given Name | R. M. |
| | Prefix | |
| | Suffix | |
| | Division | Mechanical Engineering Department |
| | Organization | University of California |
| | Address | Santa Barbara, CA, 93106, USA |

Abstract

Bree Interaction Diagrams have long been one of the major visual design guides for employing and evaluating shakedown in engineering applications. These diagrams provide representations of the realms in which elastoplastic behaviors, including shakedown, are found for a material and structure under variable loads. The creation of these diagrams often relies upon some combination of upper or lower bound shakedown theorems and numerical shakedown limit determination techniques. Part of the utility of these diagrams is that, for a given structure and loading conditions, inspecting them is sufficient to determine whether shakedown will occur or not. The diagrams cannot however, give the designer insight into how the conditions for shakedown are met. This chapter presents some graphical interpretations of one of the common methods for shakedown determination: the use of Melan's Lower Bound Theorem. The intent is to provide additional insight for designers regarding how shakedown conditions are satisfied. In this way, additional directions for modifying designs to recover shakedown behavior may also be identified. Revisiting this well-established theorem from a graphical and pedagogical approach, also provides a foundation for interdisciplinary innovation. The particular focus is on simple examples that highlight ways in which Melan's theorem may be applied to shakedown design problems.

Some Graphical Interpretations of Melan's Theorem for Shakedown Design

N. Vermaak, M. Boissier, L. Valdevit and R. M. McMeeking

1 **Abstract** Bree Interaction Diagrams have long been one of the major visual design
2 guides for employing and evaluating shakedown in engineering applications. These
3 diagrams provide representations of the realms in which elastoplastic behaviors,
4 including shakedown, are found for a material and structure under variable loads.
5 The creation of these diagrams often relies upon some combination of upper or
6 lower bound shakedown theorems and numerical shakedown limit determination
7 techniques. Part of the utility of these diagrams is that, for a given structure and
8 loading conditions, inspecting them is sufficient to determine whether shakedown
9 will occur or not. The diagrams cannot however, give the designer insight into how
10 the conditions for shakedown are met. This chapter presents some graphical inter-
11 pretations of one of the common methods for shakedown determination: the use
12 of Melan's Lower Bound Theorem. The intent is to provide additional insight for
13 designers regarding how shakedown conditions are satisfied. In this way, additional
14 directions for modifying designs to recover shakedown behavior may also be iden-
15 tified. Revisiting this well-established theorem from a graphical and pedagogical
16 approach, also provides a foundation for interdisciplinary innovation. The particular
17 focus is on simple examples that highlight ways in which Melan's theorem may be
18 applied to shakedown design problems.

N. Vermaak (✉) · M. Boissier
Department of Mechanical Engineering and Mechanics, Lehigh University,
Bethlehem, PA 18015, USA
e-mail: vermaak@lehigh.edu

M. Boissier
e-mail: mathilde.boissier@polytechnique.org

L. Valdevit
Department of Mechanical and Aerospace Engineering, University of California,
Irvine, CA 92697, USA
e-mail: valdevit@uci.edu

R.M. McMeeking
Mechanical Engineering Department, University of California,
Santa Barbara, CA 93106, USA
e-mail: rmcm@engineering.ucsb.edu

© Springer International Publishing AG 2018
O. Barrera et al. (eds.), *Advances in direct methods for materials
and structures*, DOI 10.1007/978-3-319-59810-9_11

1

1 Introduction

While shakedown concepts, limit theorems, and numerical methods have been developed since the 1920s and 1930s [1–5], their widespread acceptance and application in engineering design communities remains limited [5]. Some of the factors that would promote more widespread use of shakedown concepts and limit theorems include improving awareness through educational materials, more experimental validation efforts, and enhanced communication of shakedown benefits to different design communities. This chapter presents graphical interpretations of shakedown concepts with the intent to provide additional insight and understanding while complementing existing graphical shakedown design tools.

Within the context of plastic design under variable loads, shakedown limit theorems have been used in applications ranging from: vessels for demilitarization of munitions [6], tribology [7], multilayer semiconductor devices [8], pavement design [9, 10], shape memory alloy components [11–13], to nuclear pressure vessels [5]. The theorems delineate the boundaries between reliable and inadmissible behaviors [14–17] (see top of Fig. 1). The theorems often replace traditional yield-limited assessments of structural integrity and can be used in the design process to evaluate a structure’s response to unanticipated loads. The operational space is extended by allowing *shakedown* to occur, whereby stresses locally exceed the yield strength of a material in the first few cycles of load and thereafter, fully elastic response is recovered.

More generally, the range of possible structural responses is often illustrated through the use of a Bree Interaction Diagram, which indicates combinations of loads that lead to various material and structural behaviors. Figure 1 illustrates the classic Bree diagram for a thin-walled cylinder (with a radius, R and thickness, t), subjected to a fixed internal pressure and a cyclic radial temperature difference [14]. The ordinate is $\Delta T/\Delta T_o$, where ΔT_o is the temperature difference required for yield initiation (σ_Y) in the absence of a mechanical load ($\Delta T_o = 2(1 - \nu)\sigma_Y/E\alpha$); the abscissa is P/P_o with P_o being the pressure that causes yielding in the absence of a temperature gradient ($\sigma_Y = P_o R/t$). E , α , ν are the material Young’s modulus, coefficient of thermal expansion, and Poisson’s ratio, respectively. The elastic domain is defined by $P/P_o + \Delta T/\Delta T_o < 1$. At one extreme, wherein $P/P_o > 1$, *plastic collapse* occurs on the first load cycle, i.e. the thin wall experiences complete yielding. For intermediate combinations of P and ΔT , one of three behaviors is obtained (Fig. 1) [18]. (i) In the *shakedown* regime, localized plastic deformation that occurs in the early stages of cycling gives rise to residual stresses that stabilize the plastic response. Purely elastic behavior results during any further loading cycles. (ii) *Alternating plasticity* occurs by loading beyond the shakedown limit. Here the plastic strain increment obtained during the first half of each loading cycle is balanced by a plastic strain increment of equal magnitude but opposite sign during the second half of the loading cycle. No net strain accrues during each cycle but the structure ultimately fails by low-cycle fatigue. (iii) *Ratchetting* refers to the condition in which a net increment of plastic strain accumulates during each cycle, eventually causing rupture.

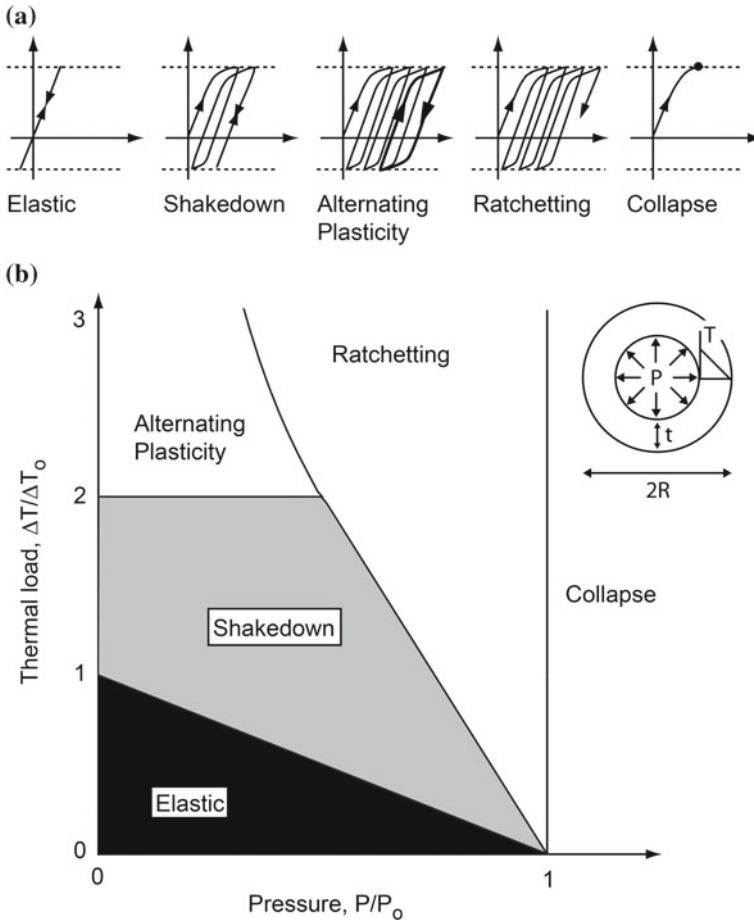


Fig. 1 **a** Prototypical stress-strain behaviors for an elastic-plastic material in the classic Bree problem and **b** the corresponding analytic Bree diagram. A cylindrical vessel is subject to constant internal pressure and a cyclic thermal gradient through the wall thickness

62 The creation of these diagrams often relies upon some combination of upper or
 63 lower bound shakedown theorems and numerical shakedown limit determination
 64 techniques. The utility of interaction diagrams such as Fig. 1 is immediately appar-
 65 ent; for an engineering application, designers may easily assess the benefits of allow-
 66 ing shakedown to occur. The interaction diagrams cannot however, give the designer
 67 insight into how the conditions for shakedown are met. This chapter presents some
 68 graphical interpretations of one of the common methods for shakedown determina-
 69 tion: the use of *Melan's Lower Bound Theorem* under small deformation theory
 70 assumptions (from Koiter [19]):

71 If any time-independent distribution of residual stresses, $\bar{\rho}_{ij}$, can be found such that the sum
 72 of these residual stresses and the “elastic” stresses, σ_{ij}^e , is a safe state of stress $\sigma_{ij}^e + \bar{\rho}_{ij} = \sigma_{ij}^s$,
 73 *i.e.* a state of stress inside the yield limit, at every point of the body and for all possible
 74 load combinations within the prescribed bounds, then the structure will shake down to some
 75 time-independent distribution of residual stresses (usually depending on the actual loading
 76 program), and the response to subsequent load variations within the prescribed limits will
 77 be elastic. On the other hand, shakedown is impossible if no time-independent distribution
 78 of residual stresses can be found with the property that the sum of the residual stresses and
 79 “elastic” stresses is an allowable state of stress at every point of the body and for all possible
 80 load combinations.

81 In other words, to assure that a structure will shakedown, one has to find a resid-
 82 ual stress field, ρ , that satisfies the following three conditions: (i) it has to be self-
 83 equilibrating, (ii) it has to be time-independent, and (iii) it has to remain within the
 84 yield limit when combined with any fictitious “elastic” stress caused by a load com-
 85 bination from the loading domain. This powerful theorem gives a necessary and
 86 sufficient condition to determine if a structure will shakedown or not. One of the
 87 major advantages of this theorem and this kind of “Direct Method” is that informa-
 88 tion about the loading path in an arbitrarily complex loading space is not needed.
 89 Rigorous bounds and shakedown predictions can be made based on purely elastic
 90 solutions or simplified elastoplastic calculations [19–31]. In contrast, the “classical
 91 load history approach” follows the incremental or step-by-step evolution of a system
 92 and finds the actual residual stress field that would result from the actual loading
 93 history that is deterministically known. Direct Methods, which historically devel-
 94 oped out of necessity and without access to computational tools, typically take a
 95 more mathematical approach to predict shakedown response [5]. It should be noted
 96 that “classical incremental or load history approaches” and “direct methods” are not
 97 competing methods, but rather complementary as each provides different informa-
 98 tion and functionality and they often have separate domains of applicability. For
 99 example, direct methods avoid cumbersome incremental load-history based calcula-
 100 tions and are especially useful when the exact loading history within a domain
 101 is unknown. Whereas the load-history based approaches provide the often crucial
 102 evolution of local quantities.

103 Several versions of proofs of Melan’s lower bound theorem can be found in the
 104 literature [19–21, 32] and many extensions of this theorem have been made to ana-
 105 lyze temperature or time-dependent properties, creep, damage, and others [5, 33,
 106 34]. Many ways to implement Melan’s theorem to determine shakedown behav-
 107 ior or shakedown limit loads have also been developed; see Weichert and Ponter
 108 [5] for a broad historical survey. One way to think about the techniques for lower-
 109 bound shakedown determination is by emphasizing “any” in the first part of the
 110 limit theorem (“*If any time-independent distribution of residual stresses, $\bar{\rho}_{ij}$, can*
 111 *be found...*”). How could one find appropriate residual stress fields? Direct methods
 112 exploit the mathematical freedom available by searching for “any” residual stress
 113 field that meets the specified shakedown conditions; to do this, direct methods use a
 114 variety of procedures from graph theory to optimization [22, 35–43].

115 In this work, two different direct method implementations of Melan's theorem for
 116 shakedown determination are considered. The goal is to illustrate graphically what
 117 is mathematically determined when an admissible residual stress field, ρ , is sought
 118 and the conditions for a structure to shakedown are met. The graphical interpreta-
 119 tions also provide a way to understand the role of key parameters and features in the
 120 shakedown determination process. Revisiting this well-established theorem from a
 121 graphical and pedagogical approach, also provides a foundation for interdisciplinary
 122 innovation. In the following, Sect. 2 will present the background and assumptions of
 123 the problems analyzed. Sections 3 and 4 present several examples. Discussion of the
 124 assumptions and limitations is presented in Sect. 5 and followed by conclusions.

125 2 Setting of the Problem

126 Consider an elastic-perfectly-plastic solid, Ω , under small deformation theory
 127 assumptions. Its boundary, $\partial\Omega$, characterized by its normal, \underline{n} , can be described in
 128 parts (Fig. 2): $\partial\Omega_0$ is the part of the boundary on which displacement is imposed,
 129 $\partial\Omega_F$ is the part of the boundary on which any traction, F , from the prescribed load-
 130 ing domain, L (Fig. 3), could be applied, and Γ is the part of the boundary that is
 131 traction-free. These parts satisfy the conditions:

$$132 \quad \begin{aligned} \partial\Omega &= \partial\Omega_0 \cup \partial\Omega_F \cup \Gamma, \\ \partial\Omega_0 \cap \partial\Omega_F &= \emptyset, \quad \partial\Omega_0 \cap \partial\Gamma = \emptyset, \quad \partial\Omega_F \cap \partial\Gamma = \emptyset. \end{aligned} \quad (1)$$

133 In the following, a constant scalar yield stress, σ_Y , is considered and a von Mises yield
 134 function, f , is adopted. As a result of a load, P , applied to a solid, Ω , on the part $\partial\Omega_F$,
 135 two types of stresses will be distinguished: (i) the *actual stresses*, σ_{actual}^P , these are the
 136 elastoplastic stresses that would be caused by the load (under the elastic-perfectly-
 137 plastic model); (ii) the *fictitious "elastic" stresses*, $\sigma_{e,fict}^P$, these are the stresses that
 138 would be caused by the load if the response were purely elastic.

Fig. 2 Schematic of structure and problem parameters

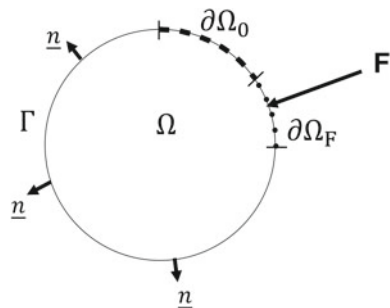
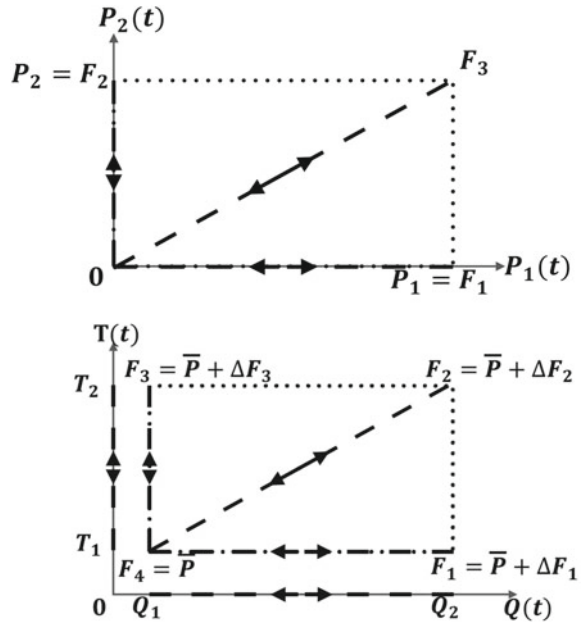


Fig. 3 Loading domains, L 

139 Lastly, the loading domain, L , assumed (Fig. 3) contains every possible loading
 140 ing combination for the loads applied to the solid. By assuming that L is a convex
 141 N -dimensional polyhedron [44], it is possible to define the loading corners,
 142 F_i , ($i \in \llbracket 1, NC \rrbracket$ where NC is the number of corners) of the loading domain, and
 143 every loading path that connects one corner to another will remain inside the loading
 144 domain. Note that all problems considered involve loading by tractions, forces or
 145 displacements and no thermal stresses are considered. We therefore keep tempera-
 146 ture constant and uniform throughout the examples presented. As a result, two types
 147 of loading domains, L , can be considered: only cyclic loads and combined cyclic
 148 and constant loads (Fig. 3). For example, at the bottom of Fig. 3, a combined cyclic
 149 and constant loading domain is illustrated. It is composed of the loads $Q(t)$ (cycling
 150 between Q_1 and Q_2) and $T(t)$ (cycling between T_1 and T_2). It should be noted that for
 151 this analysis, the constant load, \bar{P} , will be restricted to cause purely elastic response
 152 in the structure, so that the actual stress it causes is equivalent to the fictitious “elastic”
 153 stress.

154 For the remainder of this work and using the translations and adaptations of Koiter,
 155 Symonds, and König [3, 4, 19, 20, 32], the following formulation of Melan’s
 156 lower bound shakedown theorem is adopted: A solid, Ω (Fig. 2), which is subjected
 157 to any cyclic traction F , from the loading domain L , (Fig. 3) on a part $\partial\Omega_F$ of its
 158 boundary $\partial\Omega$, will shakedown under this loading domain if one can find any residual
 159 stress field, ρ , which:

- 160 • *Condition 1 (spatial)* is self-equilibrating, meaning that its divergence over the
 161 solid, Ω , is zero and the field satisfies the prescribed traction-free conditions on
 162 the solid's boundary, $\partial\Omega_F \cup \Gamma$ (with the normal, \underline{n} , Fig. 2) [21]:

$$\begin{aligned} \text{div}(\underline{\rho}) &= 0 & \text{in } \Omega, \\ \underline{\rho} \cdot \underline{n} &= 0 & \text{on } \partial\Omega_F \cup \Gamma. \end{aligned} \quad (2)$$

- 164 • *Condition 2 (pointwise)* is time-independent, meaning that its value at each point
 165 does not depend on the applied loading corner, F_i ($\forall i \in \llbracket 1, NC \rrbracket$), in the loading
 166 domain L , (note that $\underline{\rho}_i$ is the field corresponding to loading corner, F_i):

$$\forall i \in \llbracket 1, NC \rrbracket, \quad \underline{\rho}_i = \underline{\rho}. \quad (3)$$

- 168 • *Condition 3 (pointwise)* will generate a safe state of stress at each point, \underline{x} , in the
 169 solid ($\underline{x} \in \Omega$) when it is added to a fictitious “elastic” stress $\sigma_{e, \text{fict}}^{F_i}$, associated with
 170 any of the loading corners, F_i ($\forall i \in \llbracket 1, NC \rrbracket$), in the loading domain L . For a yield
 171 function, f , and a yield stress, σ_Y , this gives:

$$\forall \underline{x} \in \Omega, \quad \forall i \in \llbracket 1, NC \rrbracket, \quad f(\underline{\rho}(\underline{x}) + \sigma_{e, \text{fict}}^{F_i}(\underline{x}), \sigma_Y) \leq 0. \quad (4)$$

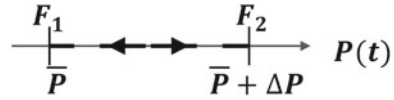
173 The conditions have been labeled as pointwise or spatially-dependent (spatial) to
 174 highlight differences for use in the following sections. Unlike Conditions 2 and 3
 175 which only have to be satisfied at each point, Condition 1 links all of the points in
 176 the solid together through the divergence term and the boundary conditions.

177 3 Graphical Interpretations of Shakedown Determination 178 with Simplified Elastoplastic Analysis

179 One approach to finding appropriate residual stress fields for use in Melan's theorem
 180 is to use simplified elastoplastic analysis [22–31]. Instead of incrementally follow-
 181 ing an entire cyclic loading history, a single elastoplastic analysis for one cycle that
 182 includes both loading and unloading could be used to calculate a representative resid-
 183 ual stress field, $\underline{\rho}$, developed in a solid, Ω . Then, the residual stress field, $\underline{\rho}$, is checked
 184 so that when it is added to the fictitious “elastic” stresses that would be caused by
 185 the same loading process, the sum will remain below the yield level. For more than
 186 one cyclic load application (or more than one cyclic load combined with constant
 187 loads), the time-independent condition (Eq. 3) is not automatically satisfied. For the
 188 following examples, simplified two-corner loading domains (Fig. 4) will be used so
 189 that only one path—the one connecting the two corners—has to be analyzed.

190 In this shakedown determination with a simplified elastoplastic analysis approach,
 191 a first step is to compute the residual stress field from loading and unloading the solid,
 192 and verify that the self-equilibrating condition is met (Eq. 2). First, the constant load,

Fig. 4 Loading domain



193 \bar{P} , is applied; this elicits an actual stress which is also the fictitious “elastic” stress
 194 (Sect. 2): $\sigma_{actual}^{\bar{P}} = \sigma_{e,fict}^{\bar{P}}$. At this stage, the load applied to the structure is the load
 195 corresponding to the first loading corner, $\bar{P} = F_1$. Then, the cyclic load ΔP is applied
 196 and the structure is fully loaded (the sum of the constant load, \bar{P} and the extremum
 197 value of the cyclic load, ΔP). This corresponds to the second loading corner, F_2 . The
 198 stress, $\sigma_{actual}^{\bar{P}+\Delta P}$, is now different from the fictitious “elastic” stress, $\sigma_{e,fict}^{\bar{P}+\Delta P}$. This new
 199 fictitious “elastic” stress, $\sigma_{e,fict}^{\bar{P}+\Delta P}$, can be related to the stress caused by the constant
 200 load, $\sigma_{e,fict}^{\bar{P}}$ (linearly elastic): $\sigma_{e,fict}^{\bar{P}+\Delta P} = \sigma_{e,fict}^{\bar{P}} + \sigma_{e,fict}^{\Delta P}$.

201 The residual stress field, ρ , is computed by completely unloading the solid: the
 202 total fictitious “elastic” stress, $\sigma_{e,fict}^{\bar{P}+\Delta P}$ is subtracted from the total stress, $\sigma_{actual}^{\bar{P}+\Delta P}$:

$$203 \quad \rho = \sigma_{actual}^{\bar{P}+\Delta P} - \sigma_{e,fict}^{\bar{P}+\Delta P}. \quad (5)$$

204 The residual stress field, ρ , by definition, is automatically self-equilibrating as
 205 demonstrated in the following. The stress field, $\sigma_{actual}^{\bar{P}+\Delta P}$, resulting from the applied
 206 load $\bar{P} + \Delta P$, satisfies the equilibrium equations (see Fig. 2):

$$207 \quad \begin{aligned} \operatorname{div}(\sigma_{actual}^{\bar{P}+\Delta P}) &= 0 \quad \text{in } \Omega \\ \sigma_{actual}^{\bar{P}+\Delta P} \cdot \underline{n} &= \bar{P} + \Delta P \quad \text{on } \partial\Omega_F \\ \sigma_{actual}^{\bar{P}+\Delta P} \cdot \underline{n} &= 0 \quad \text{on } \Gamma \end{aligned} \quad (6)$$

208 The fictitious “elastic” stress field, $\sigma_{e,fict}^{\bar{P}+\Delta P}$, satisfies the same equations, as it is the
 209 stress induced by the same loading, $\bar{P} + \Delta P$, but assuming purely elastic behavior:

$$210 \quad \begin{aligned} \operatorname{div}(\sigma_{e,fict}^{\bar{P}+\Delta P}) &= 0 \quad \text{in } \Omega \\ \sigma_{e,fict}^{\bar{P}+\Delta P} \cdot \underline{n} &= \bar{P} + \Delta P \quad \text{on } \partial\Omega_F \\ \sigma_{e,fict}^{\bar{P}+\Delta P} \cdot \underline{n} &= 0 \quad \text{on } \Gamma \end{aligned} \quad (7)$$

211 Since the divergence and the scalar product are linear operators, the nullity of the
 212 divergence of the residual stress field and the traction-free conditions are ensured
 213 by:

$$\begin{aligned}
 \text{div}(\boldsymbol{\rho}) &= \text{div}(\boldsymbol{\sigma}_{actual}^{\bar{P}+\Delta P}) - \text{div}(\boldsymbol{\sigma}_{e,fict}^{\bar{P}+\Delta P}) = 0 \quad \text{in } \Omega \\
 \boldsymbol{\rho} \cdot \underline{n} &= \boldsymbol{\sigma}_{actual}^{\bar{P}+\Delta P} \cdot \underline{n} - \boldsymbol{\sigma}_{e,fict}^{\bar{P}+\Delta P} \cdot \underline{n} = \bar{P} + \Delta P = 0 \quad \text{on } \partial\Omega_F \\
 \boldsymbol{\rho} \cdot \underline{n} &= \boldsymbol{\sigma}_{actual}^{\bar{P}+\Delta P} \cdot \underline{n} - \boldsymbol{\sigma}_{e,fict}^{\bar{P}+\Delta P} \cdot \underline{n} = 0 \quad \text{on } \Gamma
 \end{aligned} \tag{8}$$

As the solid, Ω , is elastic-perfectly-plastic, the stress, $\boldsymbol{\sigma}_{actual}^{\bar{P}+\Delta P}$, cannot go beyond the yield limit. One only needs to check that the residual stress field is “safe”, meaning that at each point, the residual stress remains below the yield level. In order to illustrate this approach for shakedown determination and gain more insight from a design perspective, a graphical interpretation is presented.

3.1 Example for Combined Cyclic and Constant Loading

Consider a two-component stress state and a von Mises yield function represented as a circle in a S_1, S_2 plane. In this plane, adding and removing stresses can be represented by adding and subtracting vectors; S_1, S_2 are stress components and the plane is not necessarily in principal stress axes. Once the stresses, $\boldsymbol{\sigma}_{actual}^F(\underline{x})$, reach the yield limit, they remain at yield on the circle until unloading. For the illustrations presented, only abstract schematic representations are used.

It has been shown above that the residual stress is self-equilibrating. Before considering the following step, a modified stress field, $\tilde{\boldsymbol{\rho}}$, is defined for convenience as the sum of the residual stress field ($\boldsymbol{\rho}$, Eq. 5) with the fictitious “elastic” stress caused by the constant load only, $\boldsymbol{\sigma}_{e,fict}^{\bar{P}}$. This stress is the one remaining in the solid, Ω , after only unloading the cyclic load ΔP :

$$\tilde{\boldsymbol{\rho}} = \boldsymbol{\rho} + \boldsymbol{\sigma}_{e,fict}^{\bar{P}} \tag{9}$$

The time-independence condition is also automatically satisfied. Once computed, the residual stress ($\boldsymbol{\rho}$, Eq. 5) will not change. Finally, the safe-state condition has only to be checked for the loading corners, at each point, \underline{x} , in the solid. For $F_1 = \bar{P}$:

$$\forall \underline{x} \in \Omega, \quad f(\boldsymbol{\rho}(\underline{x}) + \boldsymbol{\sigma}_{e,fict}^{\bar{P}}(\underline{x}), \boldsymbol{\sigma}_Y) \leq 0 \tag{10}$$

and for $F_2 = \bar{P} + \Delta P$:

$$\forall \underline{x} \in \Omega, \quad f(\boldsymbol{\rho}(\underline{x}) + \boldsymbol{\sigma}_{e,fict}^{\bar{P}+\Delta P}(\underline{x}), \boldsymbol{\sigma}_Y) = f(\boldsymbol{\sigma}_{actual}^{\bar{P}+\Delta P}(\underline{x}), \boldsymbol{\sigma}_Y) \leq 0 \tag{11}$$

Equation 11 is automatically satisfied because the solid is elastic-perfectly-plastic. From this point, the safe-state condition must be checked for the modified stress field, $\tilde{\boldsymbol{\rho}}$, (Eq. 9).

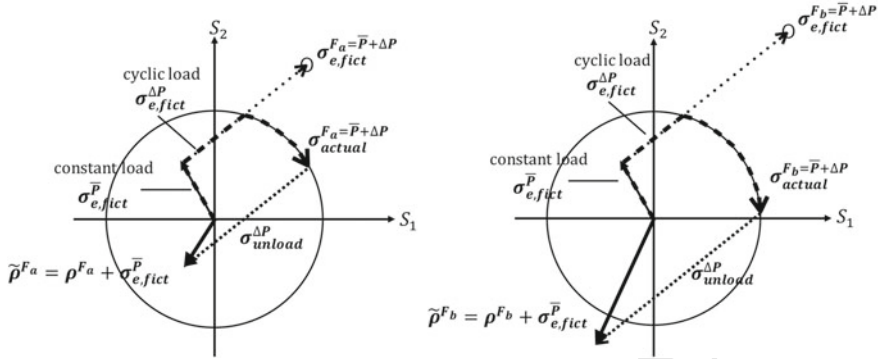


Fig. 5 Schematic illustration of direct method shakedown determination using simplified elastoplastic analysis. For a two-component stress state at a point (x) , and for a combined cyclic and constant loading case (Fig. 4): shakedown is possible (on the *left*); shakedown is **not** possible (on the *right*)

242 For a two-component stress state at a point x , Fig. 5 illustrates cases where shakedown is and is not possible. If shakedown is not possible at a single point in the
 243 structure, shakedown is prevented for the entire structure. In these figures, the *thin*
 244 *solid* lines represent the elastic stresses that result from the applied constant load
 245 $(\sigma_{e, fict}^P(x))$. Following the application of the constant load, an additional cyclic load is
 246 then applied and the resulting fictitious “elastic” stresses are shown by the *sparsely-*
 247 *dotted* $(\sigma_{e, fict}^{\Delta P}(x))$. The actual elastoplastic stresses are depicted by *thicker dashed*
 248 *lines* $(\sigma_{actual}^{F_{a,b}}(x))$ and overlap both the *sparsely-dotted* and *thin solid* lines within the elastic domain.
 249 The *thick dashed* lines for the actual elastoplastic stresses follow the yield surface (circle) when the yield limit is reached and the load is increased. Upon
 250 unloading (elastically), the fictitious “elastic” stress is subtracted from the actual
 251 elastoplastic stress $(\sigma_{actual}^{F_{a,b}}(x) - \sigma_{e, fict}^{\Delta P}(x))$. Note that only the cyclic load (and the constant load still remains.
 252 This process is represented by the *densely-dotted* line $(\sigma_{unload}^{\Delta P}(x))$. The *thick solid*
 253 *lines* show the modified stresses $\tilde{\rho}(x) = \rho(x) + \sigma_{e, fict}^P(x)$, (Eq. 9). One could argue
 254 that although the residual stress found in this way is not necessarily one that allows
 255 for shakedown to occur, it could still be possible to find another residual stress that
 256 would allow for shakedown. However, the particularity of this approach is that it
 257 gives the actual residual stress field that would be caused by the loading and unloading
 258 process. If this residual stress field does not allow for shakedown, then the structure
 259 will not shakedown. In this versatile approach, a natural ordering of the steps
 260 to check the shakedown conditions is suggested by following the physical processes
 261 of loading and unloading that the structure experiences. Many other approaches are
 262 even more divorced from physical processes and exploit the mathematical freedom in
 263 Melan’s theorem. Nevertheless, following this process could provide valuable insight
 264 for designers regarding how to recover or promote shakedown behavior.

4 Graphical Interpretations of Shakedown Determination with Purely Elastic Analysis

An example of a more mathematical implementation of Melan’s theorem uses set theory and can consider the shakedown conditions simultaneously. This kind of approach can also be used to identify new pathways to incorporate shakedown theorems in modern structural topology optimization protocols [45–49]. For the following example, a solid Ω (Fig. 2), and a cyclic loading domain, L , that includes 0 as a loading corner are analyzed (Fig. 3). For ease of understanding, the “pointwise” (time-independence and safe-state) shakedown conditions (Sect. 2) are presented together; the “spatial” (self-equilibrating) condition is applied last.

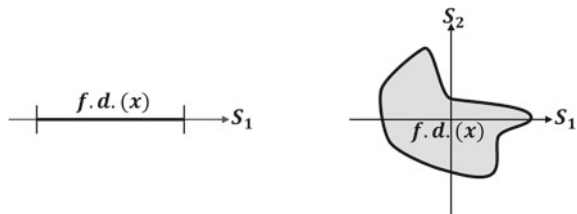
For each point, \underline{x} , in the solid ($\underline{x} \in \Omega$), a feasible stress domain (*for this point*), $f.d.(\underline{x})$, must be found, i.e. all of the stresses $\bar{s}(\underline{x})$ that, for all loading corners F_i ($\forall i \in \llbracket 1, NC \rrbracket$), satisfy the safe-state condition. The stresses, $\bar{s}(\underline{x})$, are also time-independent because they are load-independent: they do not depend on the loading corner and remain the same for the whole loading domain, L . Note that the new variable, $\bar{s}(\underline{x})$ is defined for convenience to distinguish stresses that only satisfy the pointwise shakedown conditions ($\bar{s}(\underline{x})$) from those that satisfy both the pointwise and spatial shakedown conditions (admissible residual stress fields, ρ). Then, for a point in the solid ($\underline{x} \in \Omega$), the feasible stress domain (which will be called a *feasible domain* from now on, $f.d.(\underline{x})$), is composed of the stresses, $\bar{s}(\underline{x})$, satisfying:

$$\forall i \in \llbracket 1, NC \rrbracket, \quad f(\bar{s}(\underline{x}) + \sigma_{e, \text{fict}}^{F_i}(\underline{x}), \sigma_Y) \leq 0. \tag{12}$$

For each point, the feasible domain $f.d.(\underline{x})$ can be represented in a stress coordinate system (Fig. 6). Care should be taken to ensure that the same stress coordinate system is used for all of the loading corners. Moreover, the stress coordinate system must also remain the same for the feasible domains at every point in the solid. As a result, the feasible domains, $f.d.(\underline{x})$, are not necessarily determined in principal stress axes as principal stress components depend on the applied loading and they may not be the same for each loading corner and each point in the solid.

With a feasible domain for each point in the solid, combining these domains in space will limit the admissible stress fields. The combination of feasible domains ($f.d.(\underline{x})$) gives a “feasible stress field domain” (*for the entire structure*). It is done in a space of dimension (number of stress components) + (number of spatial dimen-

Fig. 6 Schematic of a feasible domain for a point, $f.d.(\underline{x})$, with feasible stress values. *Left* example for a single stress component. *Right* example for a two-component stress



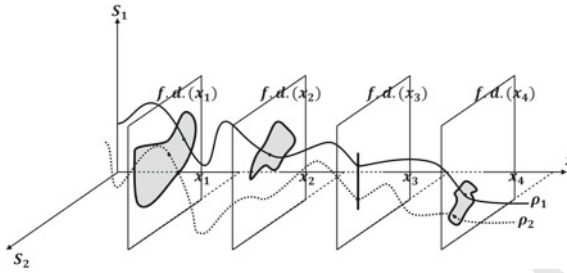


Fig. 7 Schematic illustration of the variation of feasible domains at various points in a structure. Each feasible domain, $f.d.(x)$, is drawn at the spatial coordinates of the point in the structure and extends along stress component axes (S_1, S_2). The representation of an admissible stress field, ρ , in the space of dimension (number of stress components) + (number of spatial dimensions) must remain within the boundaries set by the variation of feasible domains in the solid (i.e. the feasible stress field domain). Two possibilities for ρ are given: the example with the *solid line* (ρ_1) belongs to the feasible stress field domain whereas the example with the *dotted line* (ρ_2) does not

sions): one axis for each stress component and one axis for each spatial direction. In this space, the feasible domain for each point (x), is drawn at the spatial coordinates of the point in the solid and extends along stress component axes (Fig. 7).

To meet both the pointwise and spatial conditions (Eqs. 2–4, Sect. 2), an admissible stress field, ρ , is found in the intersection of the self-equilibrating stress fields and the feasible stress field domain. Thus, the representation of an admissible stress field, ρ , in the space of dimension (number of stress components) + (number of spatial dimensions) must remain within the boundaries set by the variation of feasible domains in the solid (i.e. the feasible stress field domain) (see schematic in Fig. 7). For ease of visualization, only the satisfaction of the divergence equation is shown; additional boundary conditions would further limit the admissible fields, ρ , within the feasible stress field domain. This “intersection of domains” approach is useful for both understanding and designing to shakedown. Modifications of the material, geometric, and problem parameters will change these two domains: reducing, enlarging, translating them and affecting the size and existence of the intersection zone in which the admissible residual stress fields, ρ , reside.

4.1 Example for only Cyclic Loading

To schematically illustrate this kind of implementation of Melan’s theorem, a four-corner cyclic loading domain, L (Fig. 3), is used. The simplified example assumes a linear yield function, f , and a one-dimensional structure, Ω , that experiences a single-component stress. To represent this problem in a continuous way, one would have to consider the pointwise shakedown conditions (Eqs. 3 and 4) at each point in the solid. In this example, only three points (x_1, x_2, x_3) are analyzed. The fictitious

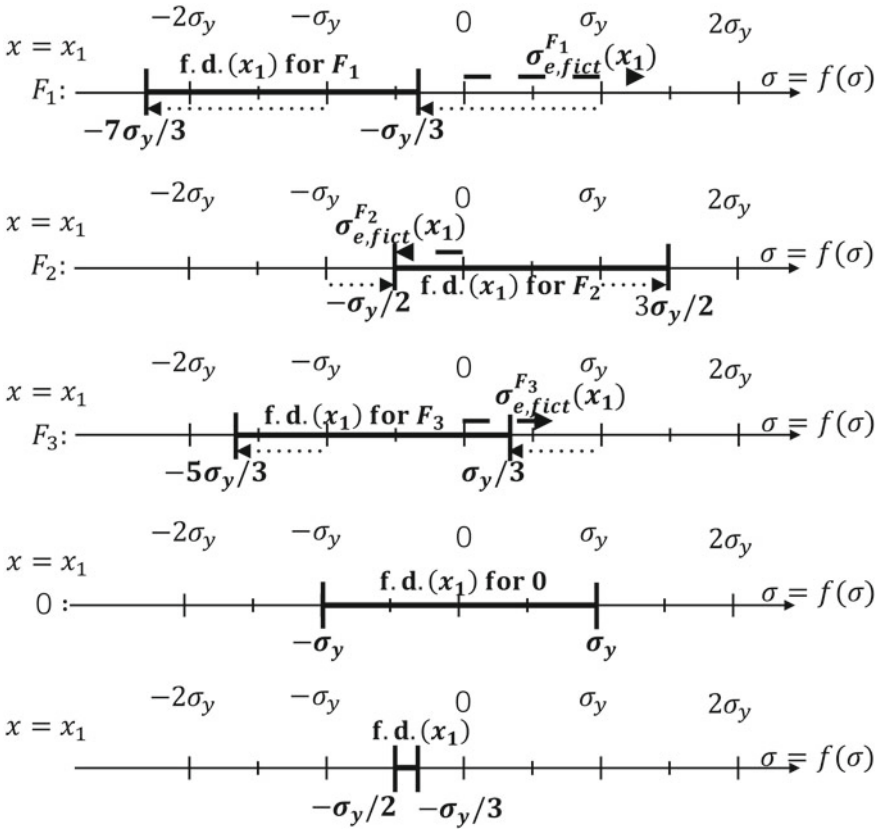


Fig. 8 Feasible domain (f.d.) for point x_1

323 “elastic” stresses caused by the loading corner (F_1, F_2, F_3 , or $F_4 = 0$), for these points
 324 in the structure are $\sigma_{e, fict}^{F_1}(x_1)$, $\sigma_{e, fict}^{F_2}(x_2)$, and $\sigma_{e, fict}^{F_3}(x_3)$.

325 A schematic case where shakedown is possible is illustrated. The feasible
 326 domains, $f.d.(x)$, at each point in the solid ($x \in \Omega$) must be computed (Figs. 8, 9
 327 and 10). These computations rely on analytical elasticity solutions or on approxima-
 328 tions using finite element analysis. For the examples below, only abstract schemat-
 329 ics are presented. The safe-state condition has to be satisfied for all four loading
 330 corners ($F_1, F_2, F_3, F_4 = 0$). The feasible domain for the points analyzed in the
 331 structure (x_1, x_2, x_3) is determined when the sum of the fictitious “elastic” stresses,
 332 $\sigma_{e, fict}^{F_1}, \sigma_{e, fict}^{F_2}, \sigma_{e, fict}^{F_3}, \sigma_{e, fict}^{F_4}$ and $\bar{s}(x)$ (Eq. 12) remain elastic.

333 Within each of the Figs. 8, 9 and 10 (and for each corresponding point x_1, x_2, x_3),
 334 there are several linear plots: one indicating the feasible domain for each of the load-
 335 ing corners ($F_1, F_2, F_3, F_4 = 0$) and a final plot that shows the feasible domain
 336 for the point (x_1, x_2 or x_3), which is the intersection of all of the feasible domains
 337 for each of the loading corners. The fictitious “elastic” stresses are computed for each

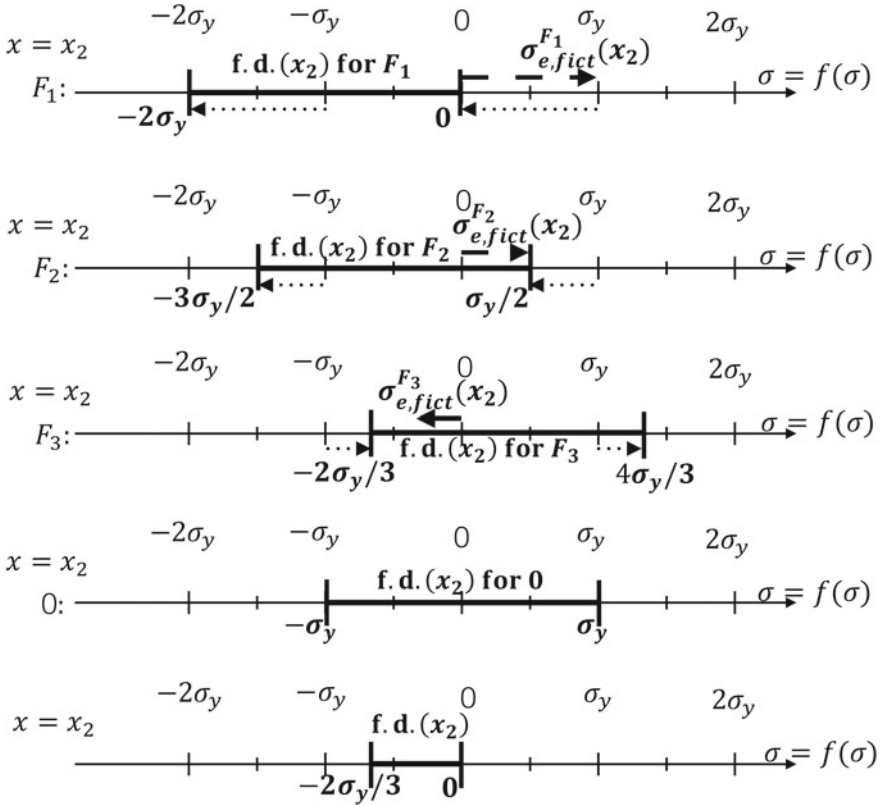


Fig. 9 Feasible domain (f.d.) for point x_2

338 loading corner and are represented by *dashed vectors* along linear stress continuums.
 339 These plots also illustrate the yielding limits (using a von Mises function $f(\sigma) = \sigma$)
 340 in tension ($\sigma = \sigma_y$) and compression ($\sigma = -\sigma_y$). The feasible domain (f.d.(x)
 341 for F_i) is represented by *thick black lines*. This domain is the translation of the elastic
 342 domain ($[-\sigma_y, \sigma_y]$) by the fictitious elastic stress ($-\sigma_{e,fict}^{F_i}(x)$), i.e. in the opposite
 343 direction and with the same magnitude. This translation is shown by the *dotted lines*
 344 at the boundaries of the elastic domain. Note that for the loading corner $F_4 = 0$, (no
 345 external loading), there are no associated fictitious elastic stresses and the translated
 346 elastic domain is the original elastic domain.

347 Combining the final feasible domains in space for each point in the structure
 348 ($\underline{x} \in \Omega$)—for example, placing them side by side along a spatial axis, allows one to
 349 visualize the limitations on the feasible stress field domain (Fig. 11). For the exam-
 350 ple presented here, it is assumed that, for points between those considered, the limits
 351 of their feasible domains will also fall linearly between the determined limits. For
 352 more general problems, finite element approximations and mesh sensitivity studies
 353 are needed. With Fig. 11, the self-equilibrating condition can be applied to find

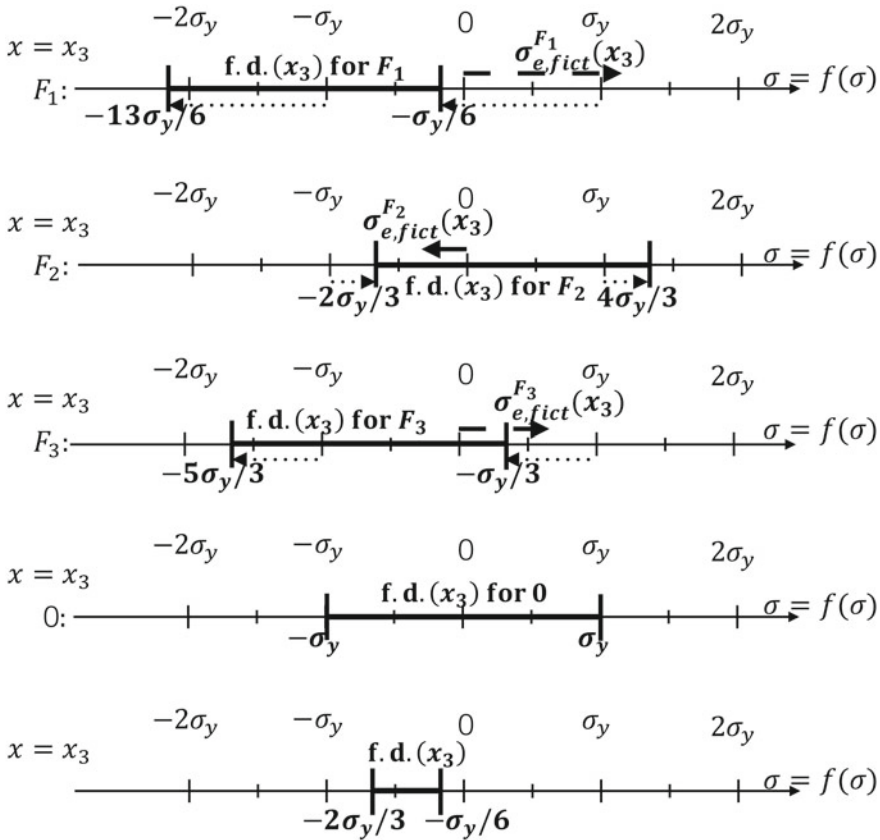


Fig. 10 Feasible domain (f.d.) for point x_3

354 the admissible stress field, ρ , (i.e. enforcing the nullity of the divergence and the
 355 traction-free state on the part of the boundary $\partial\Omega_F \cup \Gamma$):

356
$$\operatorname{div}(\rho) = \frac{\partial \rho(x)}{\partial x} = 0 \quad \text{in } \Omega, \quad \Rightarrow \quad \rho = \text{constant} \quad \text{in } \Omega. \quad (13)$$

357 For this example, the divergence equation requires one to find a constant function,
 358 ρ , which, for each point of the solid ($x \in \Omega$), would remain in the feasible domain:

359
$$\exists \rho \in \mathbb{R} \quad \text{s.t.} \quad \forall x \in \Omega, \quad \rho(x) = \rho \in f.d.(x), \quad (14)$$

360 The self-equilibrating shakedown condition (Eq. 2) does not always require a constant
 361 residual stress field ρ (Fig. 7).

362 Figure 11 shows that, for this schematic example, one can find some shakedown
 363 solutions (on the left, in the middle). In this way one assures that the whole structure,

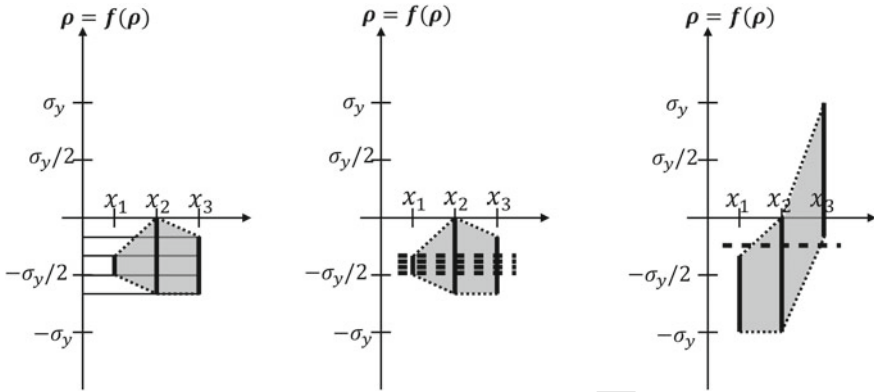


Fig. 11 *Left* feasible stress field domain from the combination of each point's feasible domain. *Middle* the same feasible stress field domain is shown with the self-equilibrating condition that indicates shakedown is possible. *Right* example of a possible feasible stress field domain where the intersection with the self-equilibrating fields is empty and shakedown is not possible

364 Ω , will shakedown under the applied loading domain, L . In contrast, one can imagine
 365 an alternative scenario for which there is no constant function (i) that will satisfy the
 366 self-equilibrating condition and (ii) that is also a member of the feasible stress field
 367 domain; thus shakedown is not possible (Fig. 11, on the right).

368 This example highlights several factors that could prevent shakedown for a structure;
 369 these factors present design opportunities to recover shakedown behavior. An
 370 empty feasible domain for a single point in the structure will prevent shakedown for
 371 the entire structure (the feasible domain for point x_1 in Figs. 8 and 9 could have been
 372 empty and then shakedown would not be possible for the structure). The feasible
 373 domain *for a point* may be empty due to the magnitude of stress levels associated with
 374 a single loading corner (i.e. greater than $2\sigma_y$ in this example), or because the
 375 combination of feasible domains for each loading corner yields an empty set when
 376 combined for the final feasible domain determination at a point. Shakedown may
 377 also be prevented due to an empty feasible stress *field* domain. This failure relates to
 378 the “spatial” self-equilibrating shakedown condition: in these examples, the condi-
 379 tion requires one to find a constant function that would remain in the feasible domain
 380 for every point in the solid (Fig. 11). As a lower bound for a structure, if it is found
 381 that shakedown is not possible for a loading corner within a given loading domain,
 382 L , then shakedown is also not possible for the entire loading domain.

383 For this kind of implementation of Melan's theorem, an example has been given
 384 to illustrate the set theory approach. It is a search for the intersection of stress fields
 385 that are admissible from pointwise and spatial-condition perspectives. It should be
 386 again emphasized that this kind of implementation does not require any elastoplastic
 387 analysis, it is based purely on elastic solutions. However, it will not provide infor-
 388 mation about the residual stress state, ρ , that actually exists in the solid. Indeed, the
 389 uniqueness of the residual stress field is derived from the load history [19] which is
 390 not considered in direct methods.

391 5 Discussion

392 The graphical interpretations and approaches presented for some implementations of
393 Melan's Lower Bound Shakedown Theorem offer tools for deeper understanding and
394 for making design choices. The mathematical processes used in methods for shake-
395 down determination are often buried in computational codes. However, as is the case
396 with many graphical representations in 2D and 3D, their practical utility is limited
397 and the graphical tools presented are not intended to replace other tools nor are they
398 recommended for complex geometries or loading domains. Nevertheless, the graphi-
399 cal tools offer complementary information to traditional Bree Interaction Diagrams.
400 Bree diagrams give bounds for elastoplastic responses (including shakedown) under
401 prescribed loading combinations but they do not indicate how shakedown condi-
402 tions are met. By elucidating how pointwise and spatial shakedown conditions are
403 met, directions for promoting and recovering shakedown behavior that are not indi-
404 cated in the Bree Diagrams may be highlighted. These may include modifications
405 of the material, geometry, and boundary conditions. Even for obvious changes such
406 as increasing the material yield strength, interaction diagrams will give the revised
407 shakedown domain, but the graphical approach and interpretations presented here
408 allow one to see how and why this parameter influences the shakedown domain from
409 a lower-bound perspective.

410 In the previous examples, several simplifying assumptions were made such as
411 ignoring the dependence of material properties (yield strength σ_y , Young's Modulus
412 E), on parameters such as temperature [33]. Including these effects would fall under
413 the pointwise conditions, modifying the shape of the feasible domain for each point.
414 In addition, in the analysis presented, only simple tractions on the boundary, cycling
415 between 0 and a maximum load have been considered. Including other loads, such
416 as volumetric loads or temperature gradients is possible but adds significant visual
417 complexity. The dimensions required to draw the feasible domains and especially the
418 combination of feasible domains for many structures are often too high for visualiza-
419 tion and defeat the purpose of these tools for understanding. Nevertheless, revisiting
420 this well-established theorem from a graphical and pedagogical approach, provides a
421 foundation for new interdisciplinary applications, including identifying pathways for
422 incorporation of shakedown in modern structural topology optimization schemes.

423 6 Conclusion

424 Several graphical interpretations of direct methods that implement Melan's lower
425 bound shakedown theorem have been developed. They serve as educational and sim-
426 ple design tools to complement existing Bree Interaction Diagrams. Where Bree
427 Diagrams give the domains of expected elastoplastic responses for a structure under
428 prescribed loading conditions, the graphical approaches developed here show how
429 and why shakedown conditions are met. They provide a graphical representation of

430 the mathematical processes at the foundation of computational shakedown codes.
 431 They also provide design insight by highlighting directions for promoting or recover-
 432 ing shakedown behavior in structures.

433 **Acknowledgements** Dr. Vermaak would like to acknowledge that, in part, this material is based
 434 upon work supported by the Air Force Office of Scientific Research under award number FA9550-
 435 16-1-0438. The authors would also like to thank Dr. Hany Fayek Abdalla for helpful discussions
 436 about the technique in Abdalla et al. [22].

437 References

- 438 1. Grüning M (1926) Die Tragfähigkeit statisch unbestimmter Tragwerke aus Stahl bei beliebig
 439 häufig wiederholter Belastung. Springer
- 440 2. Bleich H (1932) Über die Bemessung statisch unbestimmter Stahltragwerke unter Berücksich-
 441 tigung des elastisch-plastischen Verhaltens des Baustoffes. Bauingenieur 19(20):261–266
- 442 3. Melan E (1938) Der Spannungszustand eines Mises-Henckyschen Kontinuums bei veraender-
 443 licher Belastung. Sitzber Akad Wiss 147:73–78
- 444 4. Melan E (1938) Zur Plastizität des räumlichen Kontinuums. Ing Arch 8:116–126
- 445 5. Weichert D, Ponter A (2014) A historical view on shakedown theory. In: The History of theo-
 446 retical, material and computational mechanics-mathematics meets mechanics and engineering.
 447 Springer, pp 169–193
- 448 6. Simoens B, Lefebvre M, Nickell R, Minami F (2012) Experimental demonstration of shake-
 449 down in a vessel submitted to impulsive loading. J Press Vessel Technol 134:1–6
- 450 7. Ponter A, Hearle A, Johnson K (1985) Application of the kinematical shakedown theorem to
 451 rolling and sliding point contacts. J Mech Phys Solids 33(4):339–362
- 452 8. Begley MR, Evans AG (2001) Progressive cracking of a multilayer system upon thermal
 453 cycling. J Appl Mech 68(4):513–520
- 454 9. Tao M, Mohammad LN, Nazzal MD, Zhang Z, Wu Z (2010) Application of shakedown theory
 455 in characterizing traditional and recycled pavement base materials. J Transp Eng 136(3):214–
 456 222
- 457 10. García-Rojo R, Herrmann HJ (2005) Shakedown of unbound granular material. Granular Mat-
 458 ter 7(2–3):109–118
- 459 11. Sun H, Pathak A, Luntz J, Brei D, Alexander PW, Johnson NL (2008) Stabilizing shape mem-
 460 ory alloy actuator performance through cyclic shakedown: An empirical study. In: The 15th
 461 international symposium on: smart structures and materials and nondestructive evaluation and
 462 health monitoring. International Society for Optics and Photonics, p 69300
- 463 12. Peigney M (2014) On shakedown of shape memory alloys structures. Ann Solid Struct Mech
 464 6(1–2):17–28
- 465 13. Reedlunn B, Daly S, Shaw J (2013) Superelastic shape memory alloy cables: part II–
 466 subcomponent isothermal responses. Int J Solids Struct 50(20–21):3027–3044
- 467 14. Bree J (1967) Elastic-plastic behaviour of thin tubes subjected to internal pressure and inter-
 468 mittent high-heat fluxes with application to fast-nuclear-reactor fuel elements. J Strain Anal
 469 Eng Des 2(3):226–238
- 470 15. ASME Boiler and Pressure Vessel Code (2003) ASME, New York
- 471 16. BS 5500: British standard specification for fusion welded pressure vessels (1996) British Stan-
 472 dards Institute, London
- 473 17. R5 Assessment procedure for the high temperature response of structures (1990) Nuclear Elec-
 474 tric PLC
- 475 18. Abdel-Karim M, Ohno N (2000) Kinematic hardening model suitable for ratchetting with
 476 steady-state. Int J Plast 16(3–4):225–240

- 477 19. Koiter WT (1960) General theorems for elastic-plastic solids. North-Holland Amsterdam
- 478 20. König J (1987) Shakedown of elastic-plastic structures. Elsevier, The Netherlands
- 479 21. Bower A (2009) Applied mechanics of solids. CRC Press
- 480 22. Abdalla HF, Megahed MM, Younan MYA (2007) A simplified technique for shakedown limit
- 481 load determination. Nucl Eng Des 237:1231–1240
- 482 23. Abdalla HF, Megahed MM, Younan MYA (2009) Comparison of pipe bend ratchet-
- 483 ting/shakedown test results with the shakedown boundary determined via a simplified tech-
- 484 nique. In: Proceedings of the ASME 2009 pressure vessels and piping division conference
- 485 PVP2009, pp 659–666
- 486 24. Abdalla HF, Younan MYA, Megahed MM (2011) Shakedown limit load determination for a
- 487 kinematically hardening 90° pipe bend subjected to steady internal pressures and cyclic bend-
- 488 ing moments. J Press Vessel Technol 133:051212–1–10
- 489 25. Korba A, Megahed MM, Abdalla HF, Nassar MM (2013) Shakedown analysis of 90-degree
- 490 mitred pipe bends. Eur J Mech-A/Solids 40:158–165
- 491 26. Elsaadany MS, Younan MY, Abdalla HF (2014) Determination of shakedown boundary and
- 492 failure-assessment-diagrams of cracked pipe bends. J Press Vessel Technol 136(1):011209
- 493 27. Abdalla HF (2014) Elastic shakedown boundary determination of a cylindrical vessel-nozzle
- 494 intersection subjected to steady internal pressures and cyclic out-of-plane bending moments.
- 495 Nucl Eng Des 267:189–196
- 496 28. Oda AA, Megahed MM, Abdalla HF (2015) Effect of local wall thinning on shakedown
- 497 regimes of pressurized elbows subjected to cyclic in-plane and out-of-plane bending. Int J
- 498 Press Vessels Pip 134:11–24
- 499 29. Abdalla HF (2014) Shakedown limit load determination of a cylindrical vessel-nozzle inter-
- 500 section subjected to steady internal pressures and cyclic in-plane bending moments. J Press
- 501 Vessel Technol 136(5):051602
- 502 30. Abdalla HF (2014) Shakedown boundary determination of a 90° back-to-back pipe bend sub-
- 503 jected to steady internal pressures and cyclic in-plane bending moments. Int J Press Vessels
- 504 Pip 116:1–9
- 505 31. Hafiz YA, Younan MY, Abdalla HF (2015) A proposal for a simplified assessment procedure
- 506 to api-579 standard. J Press Vessel Technol 137(3):031007
- 507 32. Symonds PS (1951) Shakedown in continuous media. J Appl Mech-Trans ASME 18(1):85–89
- 508 33. Peigney M (2014) Shakedown of elastic-perfectly plastic materials with temperature-
- 509 dependent elastic moduli. J Mech Phys Solids 71:112–131
- 510 34. Weichert D (1984) Shakedown at finite displacements; a note on Melan's theorem. Mech Res
- 511 Commun 11(2):121–127
- 512 35. Spiliopoulos KV (1997) On the automation of the force method in the optimal plastic design
- 513 of frames. Comput Methods Appl Mech Eng 141(1):141–156
- 514 36. Maier G (1969) Shakedown theory in perfect elastoplasticity with associated and nonassociated
- 515 flow-laws: a finite element, linear programming approach. Meccanica 4(3):250–260
- 516 37. Bodovillé G, de Saxcé G (2001) Plasticity with non-linear kinematic hardening: modelling and
- 517 shakedown analysis by the bipotential approach. Eur J Mech-A/Solids 20(1):99–112
- 518 38. Garcea G, Leonetti L (2013) Decomposition methods and strain driven algorithms for limit
- 519 and shakedown analysis. In: Limit state of materials and structures. Springer, pp 19–43
- 520 39. Ponter AR, Engelhardt M (2000) Shakedown limits for a general yield condition: implemen-
- 521 tation and application for a von mises yield condition. Eur J Mech-A/Solids 19(3):423–445
- 522 40. Ponter A, Chen H (2001) A minimum theorem for cyclic load in excess of shakedown, with
- 523 application to the evaluation of a ratchet limit. Eur J Mech-A/Solids 20:539–553
- 524 41. Stein E, Zhang G, König JA (1992) Shakedown with nonlinear strain-hardening including
- 525 structural computation using finite element method. Int J Plast 8(1):1–31
- 526 42. Vu D, Staat M, Tran I (2007) Analysis of pressure equipment by application of the primal-dual
- 527 theory of shakedown. Commun Numer Methods Eng 23:213–225
- 528 43. Simon JW, Weichert D (2013) Interior-point method for lower bound shakedown analysis of
- 529 von Mises-type materials. In: Limit state of materials and structures. Springer, pp 103–128

- 530 44. Wiechmann K, Stein E (2006) Shape optimization for elasto-plastic deformation under shake-
531 down conditions. *Int J Solids Struct* 43(22):7145–7165
- 532 45. Allaire G, Jouve F, Toader AM (2004) Structural optimization using sensitivity analysis and a
533 level-set method. *J Comput Phys* 194(1):363–393
- 534 46. Wang M, Wang X, Guo D (2003) A level set method for structural topology optimization.
535 *Comput Methods Appl Mech Eng* 192(1):227–246
- 536 47. Bendsoe M, Sigmund O (2004) *Topology optimization: theory, methods and applications*.
537 Springer
- 538 48. Kammoun Z, Smaoui H (2015) A direct method formulation for topology plastic design
539 of continua. In: *Direct Methods for Limit and Shakedown Analysis of Structures*. Springer,
540 pp 47–63
- 541 49. Kammoun Z, Smaoui H (2014) A direct approach for continuous topology optimization subject
542 to admissible loading. *Comptes Rendus Mécanique* 342(9):520–531

Author Queries

Chapter 11

| Query Refs. | Details Required | Author's response |
|-------------|------------------|-------------------|
| | No queries. | |

UNCORRECTED PROOF

MARKED PROOF

Please correct and return this set

Please use the proof correction marks shown below for all alterations and corrections. If you wish to return your proof by fax you should ensure that all amendments are written clearly in dark ink and are made well within the page margins.

| <i>Instruction to printer</i> | <i>Textual mark</i> | <i>Marginal mark</i> |
|--|---|---|
| Leave unchanged | ... under matter to remain | Ⓟ |
| Insert in text the matter indicated in the margin | ∧ | New matter followed by ∧ or ∧ [Ⓢ] |
| Delete | / through single character, rule or underline or ┌───┐ through all characters to be deleted | Ⓞ or Ⓞ [Ⓢ] |
| Substitute character or substitute part of one or more word(s) | / through letter or ┌───┐ through characters | new character / or new characters / |
| Change to italics | — under matter to be changed | ↙ |
| Change to capitals | ≡ under matter to be changed | ≡ |
| Change to small capitals | ≡ under matter to be changed | ≡ |
| Change to bold type | ~ under matter to be changed | ~ |
| Change to bold italic | ≈ under matter to be changed | ≈ |
| Change to lower case | Encircle matter to be changed | ≡ |
| Change italic to upright type | (As above) | ⊕ |
| Change bold to non-bold type | (As above) | ⊖ |
| Insert 'superior' character | / through character or ∧ where required | Υ or Υ under character e.g. Υ or Υ |
| Insert 'inferior' character | (As above) | ∧ over character e.g. ∧ |
| Insert full stop | (As above) | ⊙ |
| Insert comma | (As above) | , |
| Insert single quotation marks | (As above) | Ƴ or ƴ and/or Ƶ or ƶ |
| Insert double quotation marks | (As above) | ƴ or ƶ and/or Ƶ or Ʒ |
| Insert hyphen | (As above) | ⊥ |
| Start new paragraph | ┌ | ┌ |
| No new paragraph | ┐ | ┐ |
| Transpose | └┐ | └┐ |
| Close up | linking ○ characters | ○ |
| Insert or substitute space between characters or words | / through character or ∧ where required | Υ |
| Reduce space between characters or words | | ↑ |